Chapter 4: Specific events during the year 2020

Section 4.1. Western Mediterranean record-breaking storm Gloria: An integrated assessment based on models and observations

Authors: E. Alvarez-Fanjul, B. Pérez Gómez, M. de Alfonso Alonso-Muñoyerro, P. Lorente, M. García Sotillo, J. Lin-Ye, R. Aznar Lecocq, M. Ruíz Gil de la Serna, S. Pérez Rubio, E. Clementi, G. Coppini, M., García-León, M. Fernandes, J. García Valdecasas, J. M. García Valdecasas, D. Santos Muñoz, M. Y. Luna Rico, M. Mestres, R., Molina, J. Tintoré, B. Mourre, S. Masina, C. Mosso, E. Reyes, A. Santana

Statement of main outcome: The storm Gloria impacted the Spanish Mediterranean coast during the days spanning 19 to 24 January 2020. The event was record-breaking, both in terms of the associated coastal damage (estimated to be more than 200 million Euros), loss of life (14 casualties) and the unprecedented high magnitudes achieved by waves, sea level and currents. The international ocean monitoring coverage provided by CMEMS (Copernicus Marine Service) systems opened up a unique opportunity to explore in detail the dynamics of this extraordinary event. This paper consolidates previously published studies by the authors, but with unique insights relevant to the Copernicus Ocean State Report, and explores in detail this exceptional storm, describing the impact, relevance and physical evolution of the event.

Products used:

Ref. No	Product name and type	Documentation
4.1.1.	MEDSEA_ANALYSIS_FORECAST_PHY_006_013 Mediterranean Sea Physics Analysis and Forecast,	PUM: https://catalogue.marine.copernicus.eu/documents/PUM/CMEMS-MED-PUM-006-013.pdf QUID: https://catalogue.marine.copernicus.eu/documents/QUID/CMEMS-MED-QUID-006-013.pdf
4.1.2.	MEDSEA_ANALYSIS_FORECAST_WAV_006_017 Mediterranean Sea Waves Analysis and Forecast,	PUM: https://catalogue.marine.copernicus.eu/documents/PUM/CMEMS-MED-PUM-006-017.pdf QUID: https://catalogue.marine.copernicus.eu/documents/QUID/CMEMS-MED-QUID-006-017.pdf
4.1.3.	GLOBAL_ANALYSIS_FORECAST_PHY_001_024 Global Ocean 1/12° Physics Analysis and Forecast updated Daily,	PUM: https://catalogue.marine.copernicus.eu/documents/PUM/CMEMS-GLO-PUM-001-024.pdf QUID: https://catalogue.marine.copernicus.eu/documents/QUID/CMEMS-GLO-QUID-001-024.pdf
4.1.4.	IBI_ANALYSISFORECAST_PHY_005_001 Atlantic-Iberian Biscay Irish-Ocean Physics Analysis and Forecast,	PUM: https://catalogue.marine.copernicus.eu/documents/PUM/CMEMS-IBI-PUM-005-001.pdf QUID: https://catalogue.marine.copernicus.eu/documents/QUID/CMEMS-IBI-QUID-005-001.pdf
4.1.5.	INSITU_MED_NRT_OBSERVATIONS_013_035 Mediterranean Sea- In-Situ Near Real Time Observations,	PUM: https://catalogue.marine.copernicus.eu/documents/PUM/CMEMS-INS-PUM-013.pdf QUID: https://catalogue.marine.copernicus.eu/documents/QUID/CMEMS-INS-QUID-013-030-036.pdf
4.1.6	SOCIB-WMOP (Balearic Islands Coastal Observing and forecasting System – Western Mediterranean OPerational forecasting system) Model	System description: https://www.socib.es/?seccion=modelling&facility=forecast_system_description Data source: https://thredds.socib.es/thredds/catalog/operational_models/oceanographical/hydrodynamics/wmop_3d/catalog.html Scientific references: Juza et al. 2016 and Mourre et al. 2018.
4.1.7	Portus system (System of Meteorological and Oceanographic Support for Port Authorities)	System description: https://portus.puertos.es/index.html?locale=en#/ Data source: https://portus.puertos.es/index.html?locale=en#/ Scientific references: Alvarez-Fanjul et al. 2018

Supplemental data for this article can be accessed online at https://doi.org/10.1080/1755876X.2022.2095169.

4.1.1. Introduction

The storm Gloria wreaked havoc on the Spanish Mediterranean coastline. The combination of strong winds and heavy rain caused storm surge and inland flooding, leaving 14 casualties and 3 more missing. Total economic losses were estimated to be around 200 million Euros, mainly in the Catalonia and Valencia regions. The unusual weather system ruined crops, destroyed seaside infrastructures, and damaged beachfront buildings along the 518 kilometres of coastline in the Valencia region (Rodríguez et al. 2020). Storm Gloria also affected 699 km of coastline in Catalonia, as well as many parts of the Balearic Islands. For example, damage estimation near the town of Deltebre, where water penetrated 3 km inland and 3000 hectares of rice fields destroyed, was estimated in the range of 9.5 million Euros. Every beach in the Barcelona Metropolitan Area sustained the worst damage seen in the last 30 years. The insurance sector received more than 11,600 claims, worth 76 million Euros. Gandía and Valencia harbours were closed to shipping traffic. Finally, wave overtopping was the main source of problems at the Balearic Islands, where the magnitude of the storm surge was minor (Pérez-Gómez et al. 2021).

During the storm, the Portus observing and forecasting system, integrated into CMEMS, remained fully operational. All components of the observing systems (buoys, sea level gauges and HF radars) worked smoothly, recording the event without any loss of data. Additionally, several CMEMS forecasting systems, as well as others nested in them, provided insight on the evolution of the storm. This framework has given an opportunity to study the storm in detail. The primary objective of this study is to analyze this singular event in the light of data from a full and comprehensive observation and forecasting system, as well as to assess the fitness for purpose of the operational oceanography systems, revealing their strengths and limitations in describing and alerting for such extreme events.

4.1.2. Marine observing and forecasting system in the region employed in the study

The CMEMS operational global ocean analysis and forecasting system (product ref-4.1.3., Lellouche et al. 2013, 2018), the CMEMS IBI regional solution (Sotillo et al. 2021) for the European Atlantic façade (product ref-4.1.4.) and the CMEMS MedMFC (Pinardi and Coppini 2010) (product ref-4.1.5. and product ref-4.1.2) were used for exploring the impact of the storm on both sea level and currents.

The ocean impact of Gloria was additionally monitored and successfully forecast by the Portus system (product ref-4.1.7), fully integrated into CMEMS, and consisting of several integrated subsystems:

- Portus Observing subsystem (see Figure 4.1.1): consisting of (1) the Spanish Deep Water Buoy Network, formed by 15 measuring positions in open waters (Alvarez-Fanjul et al. 2003), (2) the Spanish Coastal Buoy Network, with 9 measurement positions closer to the coast, (3) the REDMAR sea-level network, composed today of 40 stations, 16 of which are on the Spanish Mediterranean coast (Pérez-Gómez 2014) and (4) the Portus HF-radar network consisting of 8 stations, 3 of them located in the Ebro Delta region, located at the core of the Gloria event. All Portus Observing subsystem data are integrated into product ref-4.1.5.
- Portus forecasting subsystem: Consisting of:
  (1) The Portus wave forecasting system, based on the WAM model (Günther et al. 1992) and formed by a four-step nesting scheme, going from 1/4° in remote Atlantic waters to 1/36° spatial resolution near the continental shelf. AEMET's Harmonie-Arome (Bengtsson et al. 2017), a non-hydrostatic convection-permitting model, in employed as forcing. The resolution is 2.5 km, and the forecast length is 48 h. To expand geographic and temporal coverage to 72 h, fields from the HRES model of the ECMWF (European Centre for Medium-Range Weather Forecasts) are used. This is a hydrostatic atmosphere global model with a resolution of 10 km.
  (2) The multi-model system named ENSURF (ENsemble SURge Forecast) has been operational in PdE since 2018. First implemented by Deltares in the North Sea for integration of operational sea level forecasts in the region, PdE combined the Nivmar system (Álvarez-Fanjul et al. 2001), a classical vertically integrated barotropic storm surge forecast system, with operational baroclinic models for the first time in 2012 (Pérez-Gómez 2014). Today, the system combines sea level from Nivmar and the CMEMS regional operational models in the region, to generate a probabilistic sea level forecast at the main harbours (Pérez González et al. 2017; Pérez-Gómez et al. 2019). ENSURF employs the Bayesian Model Average (BMA) technique (Beckers et al. 2008) to generate improved forecasts and their confidence interval at locations with tide gauges: the individual

forecasts obtained from existing operational models at a particular site are combined with different weights obtained from its performance assessment results in a recent training period (7 days in this case). This requires near-real-time access to tide gauge data and automatic quality control of these data (as required for the Nivmar system), and specific data tailoring of model outputs as will be described below. ENSURF is also a valuable operational validation tool that allows a detailed assessment of the skills of different models to forecast coastal sea levels.

- Additionally, data from the SOCIB's WMOP circulation forecasting system are also used in this study (product ref-4.1.6.). WMOP is a high-resolution ocean forecasting system implemented over the Western Mediterranean Sea. It is run operationally daily, producing 72-hour forecasts of ocean temperature, salinity, sea level and currents (Juza et al. 2016; Mourre et al. 2018). It is based on a configuration of the Regional Ocean Modelling System (ROMS, Shchepetkin and McWilliams 2005), with spatial coverage from Gibraltar strait to Sardinia Channel and Spatial resolution varying from 1.8 to 2.2 km. Boundary conditions are taken from the CMEMS Mediterranean model. Finally, SOCIB's HF radars (R4 and R5 in Figure 4.1.1) are also employed.

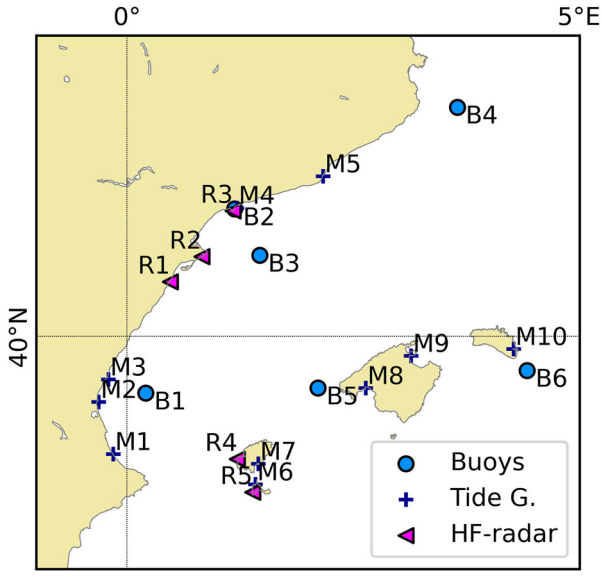

Figure 4.1.1. Portus in-situ station in the Gloria's impact region. M stands for sea level gauge, B for Buoy and R for HF-radar. Codes stand for M1-Gandía, M2-Valencia, M3-Sagunto, M4-Tarragona, M5-Barcelona, M6-Formentera, M7-Ibiza, M8-Palma de Mallorca, M9-Alcudia, R1-Vinaroz, R2-Alfacada, R3-Salou, B1-Valencia, B2-Tarragona (coastal), B3- Tarragona (deep water), B4-Begur, B5-Dragonera, and B6-Mahón. SOCIB's HF radars are marked as R4 and R5. CMEMS data product ref-4.1.5.

4.1.3. Description of the event

4.1.3.1. Synoptic description of the meteorological situation

Storm Gloria impacted the study area (Figure 4.1.1) from 19 to 24 January 2020. A surface low developed over the entire western basin (de Alfonso et al. 2021), because of the so-called Rex Block, a large-scale blocking pattern characterised by two adjacent (northern) high and (southern) low pressure systems in upper atmospheric levels (Rex 1950). Rather than the relatively deep system of low pressures over the western Mediterranean, the primary source of Gloria was the anomalously powerful anticyclone that governed central Europe, with sea level pressure exceeding 1050 hPa.

This persistent dipole was visible for the whole investigation period, following a clockwise rotation. During the first stage of the developing surface cyclone (19th–20th), an intense pressure gradient gave rise to very strong northeasterly winds (above 20 $m \cdot s^{-1}$) that affected broad areas of the eastern coast of Spain. On January 19th and 20th, wind gusts reached 108 km h^{-1} in Barx (Province of Valencia, Community of Valencia) and 115 km h^{-1} in Oliva (same province as Barx).

Afterwards, during the 21st, the atmospheric pattern evolved towards a north–south-oriented dipole, triggering a change to predominant easterlies blowing over the entire study area. The dipole-like sea level pressure structure weakened during the 22nd and mostly vanished by the 23rd, with Sea level pressure differences over the region affected by Gloria presenting values similar to pre-storm conditions. The northern high-pressure system fully dissipated by 24 January, while the weakened low remained for a few days at lower latitudes.

This extreme meteorological situation induced a strong response in the ocean, generating extreme values of the main ocean variables as shown in Figure 4.1.2, the details of which will be described in the rest of section 4.4.

4.1.3.2. Waves

Figure 4.1.3 shows the forecasted significant wave height fields provided by the Portus wave model at different times. The figures coincide with the storm peak at Dragonera (a), Valencia (b), Tarragona (c) and Begur (d). The maximum value, over 8 m, was reached in Gulf of Valencia, on January 20th (see the Complementary Material for a description of the temporal evolution).

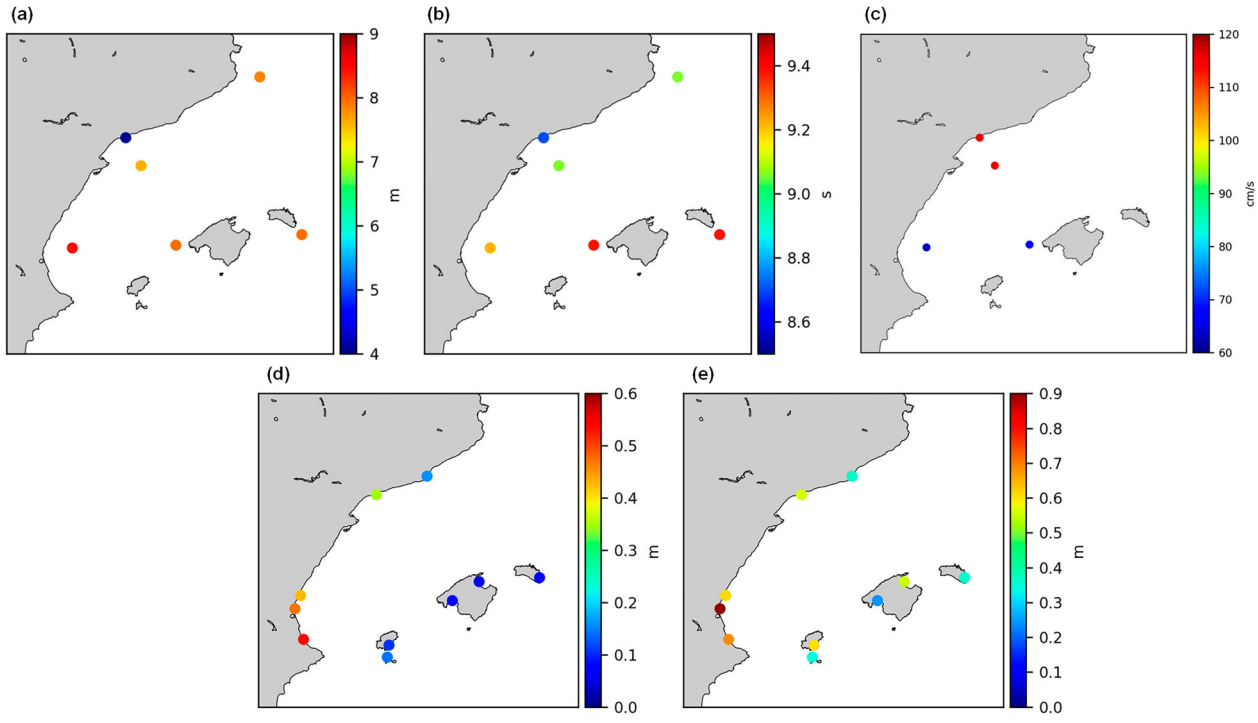

Figure 4.1.2. Maximum values recorded during the Gloria event for the different ocean variables. Upper left panel shows significant wave data, upper centre Mean wave period, upper right current speed, lower left sea level residual and lower right high frequency sea level oscillations amplitude. CMEMS data product ref-4.1.5.

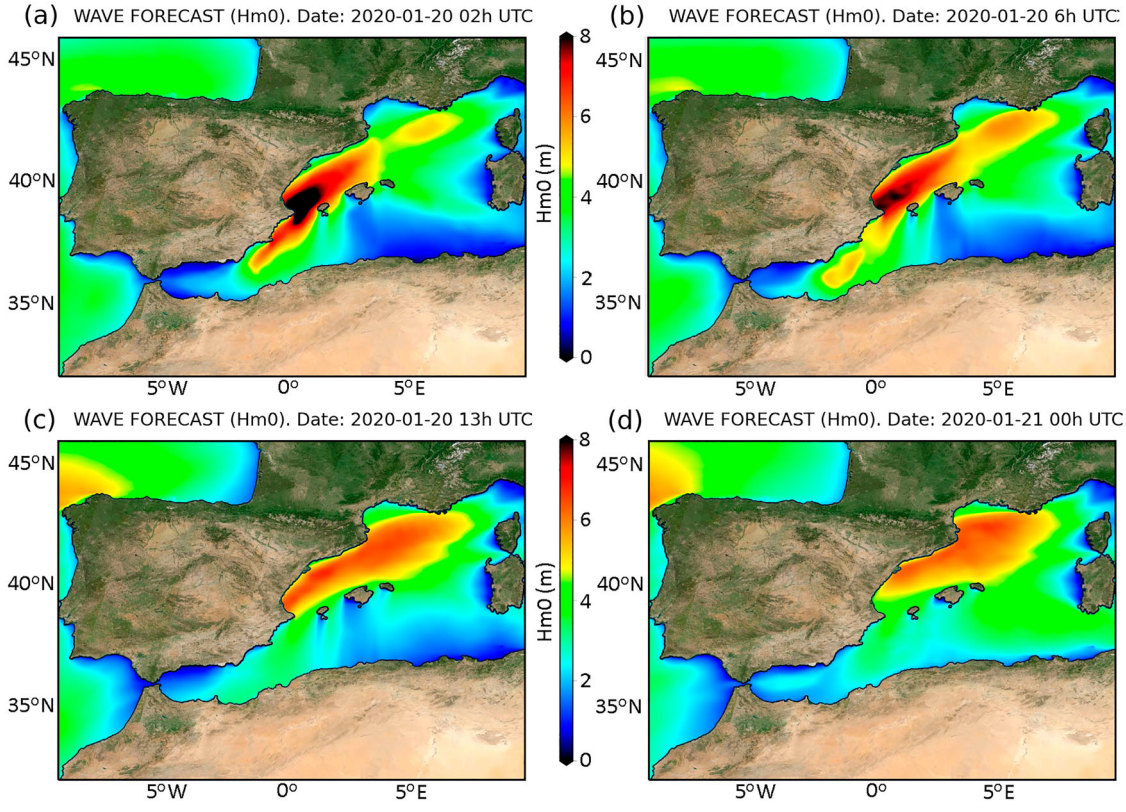

Figure 4.1.3. Map of the significant wave height field provided by the forecast wave system during Gloria at: 2020-01-20 02 UTC (a), 2020-01-20 06 UTC (b), 2020-01-20 13 UTC (c) and 2020-01-21 00 UTC (d). They coincide with the storm peak measured at Dragonera, Valencia, Tarragona and Begur respectively. Product ref-4.1.7.

The evolution of the storm is consistent with the magnitude and direction of the wind during the event. These spatial wind fields produced the highest waves (Figure 4.1.2) in the region at the north of Cape de la Nao, where the buoy M1 is located (see Figure 4.1.1). At this position, and for an along-shore wind as generated by Gloria, the whole Catalan-Balear Sea acts as an effective fetch area, explaining the location of the highest wave height observations and the exceptional long wave periods.

New records of significant wave height were observed on five of the six buoys in the region affected by the storm, on occasion with drastic increments (de Alfonso et al. 2021). The Valencia buoy's highest historical measurement increased to 8.4 m (see Figure 4.1.2) from the previous 6.2 m. The associated mean wave period (Tm02), recorded at the peak of the storm, shows extraordinarily high values. It exceeded 9 s in four of the six locations. These values set new records for the Valencia, Tarragona, Tarragona coastal and Begur buoys. At the Tarragona deep water and coastal buoys, the maximum value for Tm02 arrived some hours after the storm peak, reaching 9.1 and 8.7 s, respectively. This is consistent with previous studies of the region, where the significant wave height (Hm0), peak period (Tp) and duration present a significant interdependence (Lin-Ye et al. 2016).

Significant wave heights beat the record for duration. Significant wave height was above 5 m for 39 h, while the usual duration of such high waves is around 12 h. This was a critical factor in Gloria being so destructive. This extraordinary length is linked to the duration of the winds over the area, associated with the slow evolution of the dipole of the pressure gradient and very strong from the 19th to 22nd. Analysis of the wind maps derived from the numerical models shows that most of the Catalan-Balear Sea suffered winds over 15 m s^{-1} for a period longer of at least 50 h, and winds over 6 m s^{-1} for three consecutive days (de Alfonso et al. 2021). Mean wind regime analysis in the region shows that only around 7% of the storm events have similar durations.[1]

Portus tide gauges measure at 2 Hz frequency, monitoring waves inside the ports. During Gloria, local significant wave height Hm0 reached 2.11 m at Valencia (new historical record), 1.03 m at Gandía, 1.74 m at Tarragona and 1.36 m at Sagunto. Peak periods (Tp) were, as mentioned, very long for the area, reaching 12.89 s at Valencia and 12.68 s at Tarragona. Note that these local measurements depend strongly on the instrument location inside the harbour. Valencia, Tarragona and Sagunto are the most exposed to the open ocean wave conditions (de Alfonso et al. 2021). In any case, these high values demonstrate that wave contributions to inundation processes must be considered.

4.1.3.3. Sea level

The largest increase of sea level during Gloria was recorded at Valencia, Gandía, and Sagunto tide gauges, followed by Carboneras and Tarragona (Pérez-Gómez et al. 2021). The sea level increase was small or even negligible at the rest of ports (Balearic Islands and Barcelona) (see Figure 4.1.2), confirmed by the magnitude of the non-tidal residual. De-tiding hourly data, the surge component reached 54 cm above Mean Sea Level (MSL) at Gandía, 47 cm at Valencia, 43 cm at Sagunto, 35 cm at Tarragona and 15 cm at Barcelona. Surge values were <10 cm above MSL in the Balearic Islands (Ibiza, Palma, Alcudia, Mahón, and Formentera). Hourly total sea level achieved an historical record only at Gandía (64 cm), well above the second highest value (59 cm) recorded in 2010 (time series 2007–2020), while in Valencia and Sagunto the maximum hourly value was the third highest since 2007. Interestingly, in Barcelona, the maximum reached only 55 cm above the tide gauge datum, far from the historical records at this harbour (81.2 cm in 2019). Sea level was over the 99th percentile for at least two days at Gandía, Valencia and Sagunto.

This behaviour of sea level is consistent both with the wind fields and the current fields (see Figure 4.1.5). Theory states that the vertically integrated wind-induced transport in shelf areas tends to be more aligned with the wind than in open waters (where it is expected to be perpendicular, following Ekman's theory), due to the effect of the bottom spiral (Pugh 1996). As a result, the wind piled water in all the coastal domain south of Ebro's Delta, but particularly against Cabo de la Nao (at the M1 sea level gauge region), which became a natural barrier for water transport explaining, the maximum amplitude measured at Gandía. This also explains the much smaller surge at Barcelona and at the Balearic Islands (see Figure 4.1.2).

Apart from waves and hourly sea level, it was found that High Frequency Sea Level Oscillations (HFSLO), with periods within 30–300 s, had significant magnitude and were relevant for understanding coastal damages (Pérez-Gómez et al. 2021). Again, the Portus high frequency sampling makes such an assessment possible. Maximum HFSLO amplitude (Hmax: maximum oscillation amplitude in one hour) reached record values for the period since the installation of the new radar sensors in Valencia (90 cm), Sagunto (57 cm) and Ibiza (60 cm). Gandía and Tarragona recorded their 5th highest maximum Hmax in their time series.

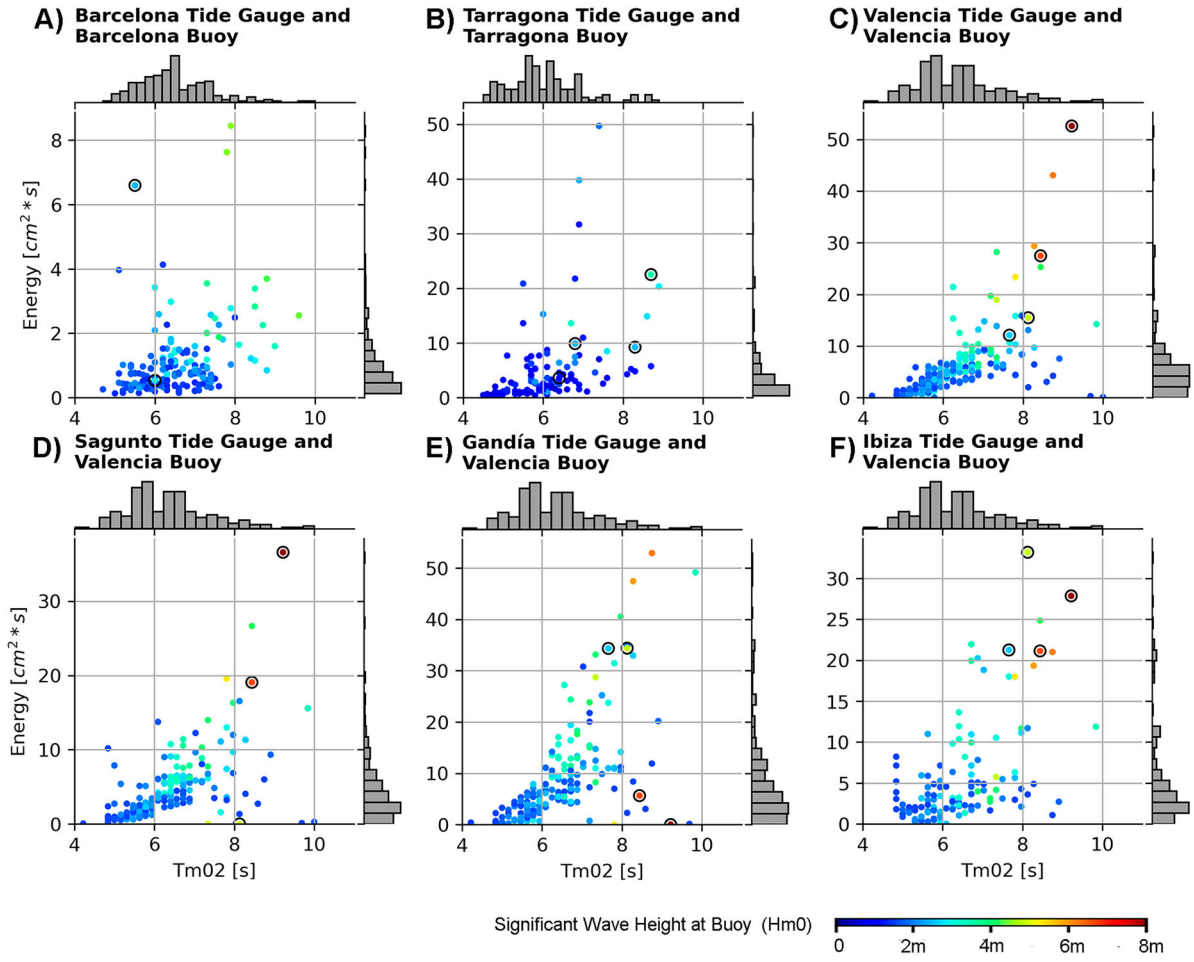

Figure 4.1.4. Infragravity band energy (30 s – 5 min band) at the tide gauge vs T_{m02} at the closest buoy for the historical tide gauges record. The historical maximum energy in this band was recorded in Valencia, Sagunto and Ibiza during Gloria (circles). Colour code represents the significant wave height. All data from product ref-4.1.5., except 2 Hz data from ref-4.1.7.

Spectral analysis of the time series shows that, during this event, the HFSLO energy was mainly concentrated in the infragravity band (30–300 s). The well-known origin of these oscillations, very frequent on the Iberian Peninsula Atlantic coast, but unnoticed before on the Mediterranean one, is transfer of energy from long period waves. This is reinforced by two facts: (1) in all cases, the energy evolution of the 30–300 s band is highly correlated in time with the height of the waves measured by the tide gauges and (2) there is a clear correlation between the presence of long wave periods and activity in the infragravity band (see Figure 4.1.4).

4.1.3.4. Currents

The circulation models illustrate the impact on the currents of the shelf region (see Figure 4.1.5 with results from the WMOP system). The winds created a strong along-shore current in the region, affecting mainly the shelf and, to a lesser extent, the slope. This pattern induced a transport that is consistent with the areas of maximum surge, as shown in Figure 4.1.2. Nevertheless, the model information about the values of the currents at a specific point and time cannot be given with the same reliability as is the case for the waves, as will be shown in the validations presented as complementary material.

The Ebro delta region is monitored by a buoy (B3 in Figure 4.1.1) with a current meter, and by HF radar stations (R1, R2 and R3 in Figure 4.1.1). Results of both systems can be seen in Figure 4.1.6. Both the HF-radar system and the deep-water buoys measured high values of sea current magnitude in the region, as a clear response to the wind. The impact of Gloria is evident on the surface maps obtained by the HF-radar (see Figure 4.1.6, upper panels). Before the arrival of Gloria, the Ligurian-Provençal-Catalan current is visible, but with moderate velocity. Observations during the event show both a perceptible intensification of the surface currents and a broadening of the strong current area, as a direct response to the intense winds. These observations are

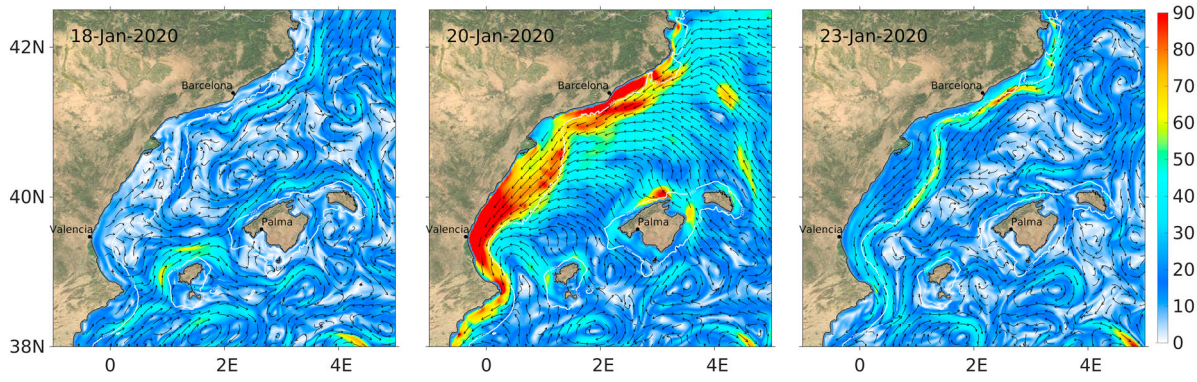

Figure 4.1.5. Daily average WMOP surface currents (cm/s) for the pre-storm (18 January 2020), storm (20 January 2020) and post-storm (23 January 2020) conditions. The arrows and the colour indicate the direction and the magnitude of the currents, respectively. Data product 4.1.6.

consistent with the model results shown in Figure 4.1.5 (see complementary material section for further considerations on the model performance).

It is remarkable that at the position near Valencia, where the B1 buoy is located, the currents generated by the model are confined to the shelf. This explains the relatively low maximum velocities observed at this position (Figure 4.1.2), since the buoy is located at the shelf break. In any case, as will be shown in the annex on models validation, the details of the solution for currents provided by the numerical models at a specific point at time must be considered with caution.

Hourly B3 buoy time series of current speed and direction were compared with HF radar data

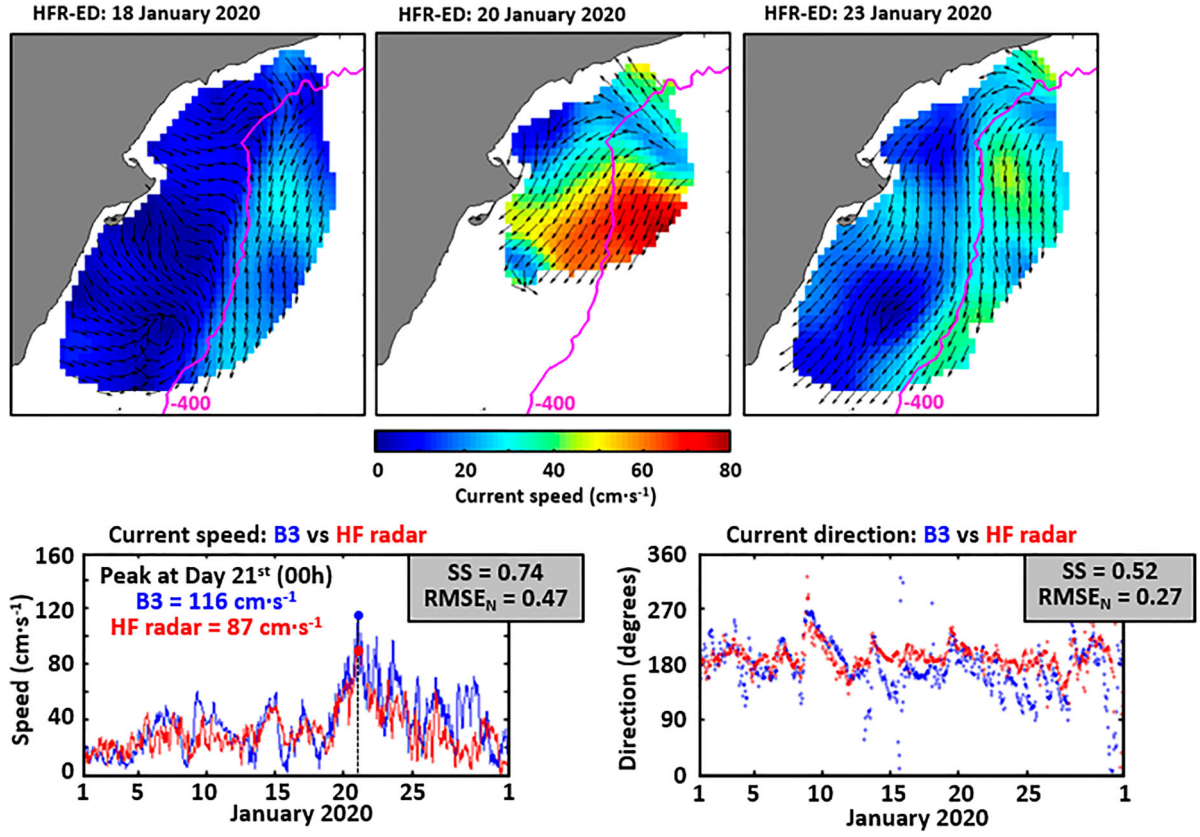

Figure 4.1.6. Upper panel shows the observations of the HF radar during Gloria event (daily means). Lower panels the comparison of hourly surface current speed (A) and direction (B) provided by B3 buoy (red) and HF radar (blue) at the closest grid point, for January 2020. CMEMS data product ref-4.1.5.

estimations at the closest grid point (see Figure 4.1.6, lower panels). Both devices captured the timing of the peak in the current speed (January 21st at 00 h), although the HF-radar undermeasured the exceptional value recorded by the Tarragona deep water buoy (116 cm s^{-1}). This measurement is over the 99.9 percentile and the 15-year historical record, previously established at 79 and 98 cm/s, respectively. Note that the highest current speed registered during another severe event in January 2017 was 53 cm.s^{-1} (half of Gloria event´s top speed), highlighting the exceptionality of Gloria.

Additionally, Gloria's effect in an adjacent area, less affected by the event as evidenced by the model results, could be seen on the anomalous surface circulation patterns measured by the HFR systems in the Ibiza Channel (R4 and R5 on Figure 4.1.3). On the 19th of January, the analysis of the HFR derived surface currents in the Ibiza Channel revealed the intensification of the surface flow (reaching 60 cm/s), with a clockwise veering from NE to SW during the storm, abruptly interrupting the well-known Balearic current (Lorente et al. 2021).

4.1.4. Discussion

The spatial coverage and temporal sampling of the ocean observing system has been exploited to monitor the impacts of the Gloria event, except in the case of the HF radar. For the latter, the low number of stations only permits monitoring of surface currents for limited regions. All available instrumentation produced timely critical data. This is a result of best practices applied on the maintenance of these instruments. Nevertheless, it is important to highlight that this is not the case for all storms. On some occasions, instrumentation is under maintenance or repair. The deep-water buoys of Puertos del Estado employed in this paper are typically available 90% of the time during a normal year. Looking at Figure 4.1.1 it is obvious that the level of spatial redundancy of the system is low, and this could have consequences. For example, one of the most important reasons to measure waves is for obtaining long time series that can be used for extreme analysis, something mandatory when designing maritime infrastructures, such as piers. Note that the cost of these public works range typically from tens to hundreds of millions of Euros. The impact of Gloria on these works is clear when computing return periods. For instance, in Valencia, the Hm0 of 8.44 m was associated with a return period of 707.7 years before Gloria but is reduced to 37.2 years when considering the new data. Similarly, in Dragonera, the Hm0 of 7.97 m (544.4 years) has changed to a new return period of 40.3 years, whereas in Tarragona, a Hm0 of 7.62 m (414.7 years) corresponds to a new return period of 48.7 years. This demonstrated that losing the data from one storm due to a malfunction of an instrument can have important consequences when designing new infrastructures, something that will affect both their construction cost and safety. Obviously, numerical modelling came as a help here to fill the gaps, but considering the costs associated with the creation and repair of coastal infrastructures, it is valuable to have reliable measurements. Additionally, a higher level of redundancy would contribute to reduce gaps in the data and, therefore, to help in the study of trends of extremes in climate change studies. Therefore, more stress should be placed in the future on the redundancy of instrumentation, even if the maintenance costs are increased.

All the forecasts and measurements were distributed to the community through the Portus web page (product ref-4.1.7.) and, in the case of the Ports, via the specific SAMOA (Sistema de Apoyo Meteorológico y Oceanográfico a las Autoridades Portuarias) service, a series of downscaled models and downstream applications designed to provide the information required for safe Port operation (Alvarez-Fanjul et al. 2018). Thanks to this information, all major Ports at Spain in the affected area took contingency actions, like closing to maritime traffic in advance, reducing the possibilities of fatal accidents. A good example of these preventive actions can be found at Barcelona Port. At this location, the SAMOA service includes an overtopping forecast service. The first overtopping alert was issued on 16 January 2020 12 h (72 h forecast), and the last overtopping alert was on 23 January 2020 00 h (12 h forecast). The overtopping was successfully predicted, with an error below 3 h of the first recorded event, within 72 h of anticipation. This gave time to the Port Police to close certain areas of the pier to pedestrians and road traffic, preventing possible accidents. It is noteworthy that the forecast horizon of 72 h was sufficient to implement mitigation actions. Real time validation of the models, based on the Portus observing component, was also important to generate confidence in the forecasting systems. During the event, and in the previous days, the real time validation system was critical to increase the confidence of the stakeholders at the Ports that, alarmed by the unprecedent forecasts, contacted Puertos del Estado, seeking additional confirmation.

Finally, the observations of the Portus system are demonstrating that climate change is also playing its

role in the devastation. According to the relative mean sea level trends obtained from Barcelona, Valencia and Ports, the overall relative sea level rise in 27 years may have reached up to 15 cm at some coastal locations of the Spanish Mediterranean coast. Over this higher mean sea level, all relevant sea level oscillations discussed here have taken place. In simpler words, the same surge magnitude would generate total extreme sea levels up to 15 cm higher today than in 1993.

In summary, this study has illustrated that local operational oceanography services in the area, providing integrated information with CMEMS services, are ready to generate useful information for decision making during extreme events. The coastal damages and human life losses produced by Gloria highlight the importance of investing in a state-of-the-art monitoring and forecasting system. In this case, international collaboration at the European level was of paramount importance, and thanks to the CMEMS service, several aspects of the storm were properly forecast, and mitigation actions were taken in advance.

Section 4.2. Oceanic response to the 2020 Siberian heatwave

Authors: V. S. Lien, S. Aaboe, E. J. Down, L. Bertino, S. Hendricks, T. Lavergne, J. Xie, A. Mangin, M. Bretagnon

Statement of main outcome: 2020 stands out as one of the years with the least sea ice in the Arctic since satellite records started in the late 1970s. For each of the months July to December, the sea-ice cover was either at its lowest or second lowest on record. Most remarkable was the one month earlier melting and one-month later freeze-up in the Kara and Laptev seas, giving rise to prolonged ice-free seas along the Siberian shelf. The sea-ice anomalies followed the record-breaking heatwave in northern Siberia. We find that anomalous, wind-driven sea-ice drift in the Laptev Sea basin in July 2020, preconditioned by anomalously thin sea ice, exposed the ocean to prolonged heating from incoming shortwave radiation. Moreover, higher surface salinities in the Laptev Sea basin due to the lack of local ice melt, combined with large SST anomalies and subsequent vertical mixing, reduced the upper 100 m water column stability by more than 50% compared with the climatological average. Consequently, 2020 has experienced a positive anomaly in primary production in the Arctic shelf regions, due to the relatively higher supply in nutrients within the surface layer, and a decrease for the global Arctic By December, the sea-ice thickness in the Laptev Sea increased to climatological values through a combination of freezing and regional convergence. Below the sea-ice cover, a reduced stability persisted in the upper 100 m of the water column.

Products used:

Ref. No	Product name and type	Documentation
4.2.1	SEAICE_GLO_SEAICE_L4_REP_OBSERVATIONS_011_009 Global Ocean sea ice concentration time series reprocessed (OSI-SAF)	PUM: http://marine.copernicus.eu/documents/PUM/CMEMS-OSI-PUM-011-009.pdf QUID: http://marine.copernicus.eu/documents/QUID/CMEMS-SI-QUID-011-001to007-009to013.pdf
4.2.2	SEAICE_GLO_SEAICE_L4_NRT_OBSERVATIONS_011_001 Global Ocean – Arctic and Antarctic – sea ice concentration, edge, type and drift (OSI-SAF)	PUM: http://marine.copernicus.eu/documents/PUM/CMEMS-SI-PUM-011-001.pdf QUID: http://marine.copernicus.eu/documents/QUID/CMEMS-OSI-QUID-011-001to007-009to012.pdf
4.2.3	SEAICE_ARC_SEAICE_L3_NRT_OBSERVATIONS_011_014	PUM: https://marine.copernicus.eu/documents/PUM/CMEMS-SI-PUM-011-014.pdf QUID: https://marine.copernicus.eu/documents/QUID/CMEMS-SI-QUID-011-001to007-009to014.pdf
4.2.4	SST_GLO_SST_L4_NRT_OBSERVATIONS_010_001. OSTIA NRT analyses	PUM: http://marine.copernicus.eu/documents/PUM/CMEMS-SST-PUM-010-001.pdf QUID: http://marine.copernicus.eu/documents/QUID/CMEMS-SST-QUID-010-001.pdf
4.2.5	ARCTIC_REANALYSIS_PHYS_002_003. Arctic MFC PHY reanalysis	PUM: http://marine.copernicus.eu/documents/PUM/CMEMS-ARC-PUM-002-ALL.pdf QUID: http://marine.copernicus.eu/documents/QUID/CMEMS-ARC-QUID-002-003.pdf
4.2.6	ARCTIC_ANALYSIS_FORECAST_PHYS_002_001_a. Arctic MFC NRT PHY forecasts	PUM: http://marine.copernicus.eu/documents/PUM/CMEMS-ARC-PUM-002-ALL.pdf QUID: http://marine.copernicus.eu/documents/QUID/

(*Continued*)